Catalytic applications of OSDA-free zeolite Beta

Trees De Baerdemaeker [a], Bilge Yilmaz [b], Ulrich Müller [c], Mathias Feyen [c], Feng-Shou Xiao [d], Weiping Zhang [e], Takashi Tatsumi [f], Hermann Gies [g], Xinhe Bao [h] and Dirk De Vos [a]*

[a] Centre for Surface Chemistry and Catalysis, KU Leuven, Kasteelpark Arenberg 23, 3001, Heverlee, Belgium;

[b] BASF Corporation, Chemicals Research and Engineering, Iselin, NJ 08830, USA;

[c] BASF SE, Chemicals Research and Engineering, 67056, Ludwigshafen, Germany;

[d] Zhejiang University, 310028, Hangzhou, China;

[e] State Key Laboratory of Fine Chemicals, Dalian University of Technology, 116024, Dalian, China;

[f] Chemical Resources Laboratory, Tokyo Institute of Technology, 226-8503, Yokohama, Japan;

[g] Institute of Geology, Mineralogy and Geophysics, Ruhr-University Bochum, 44780, Bochum, Germany;

[h] State Key Laboratory of Catalysis, Dalian Institute of Chemical Physics, 116023, Dalian, China

Corresponding author

Dirk.devos@biw.kuleuven.be

Kasteelpark Arenberg 23, Post box 2461

3001 Heverlee

Belgium

Tel: (32)16321639, fax: (32)16321998

Abstract

Zeolite Beta obtained from seeded synthesis without the use of organic structure directing agents (OSDA) has been used as a catalyst in different types of reactions. The large number of strong acid sites resulted in a high activity for the alkylation of benzene with ethene and a high cracking activity in the hydroconversion of *n*-decane. However, the high framework polarity resulted in fast deactivation in the acylation of aromatic ethers. Dealumination treatments resulted in improved stability in alkylation reactions with the more reactive olefins like propene. In acylation reactions, the activity was significantly increased and in hydroconversion, a better balance between the hydrogenation/dehydrogenation and the acid sites was obtained.

Keywords

Zeolite Beta; OSDA-free synthesis; dealumination; alkylation; acylation; hydroconversion

1. Introduction

Zeolites have a wide area of application as catalysts, adsorbents and ion exchangers [1,2]. Of the more than 200 known zeolite topologies with a framework code assigned by the Structure Commission of the International Zeolite Association [3], Beta zeolite is one of the handful of zeolite structures that constitute the majority of the commercial zeolite catalyst production. It can be used for a variety of applications, ranging from large scale processes, such as alkylations and transalkylations, to smaller scale fine chemical production [4-10]. The first synthesis of Beta zeolite was reported by Wadlinger *et al.* already in 1967 [11], but its structure, consisting of the

random intergrowth of two polymorphs was only elucidated in 1988 [12,13]. Like zeolite Y (FAU), which is one of the other important structures in commercial zeolite synthesis, Beta zeolite has a three-dimensional 12-membered ring pore structure, but its pore dimensions are slightly smaller and it lacks the supercages so typical for the FAU topology. These structural differences lead to different catalytic properties [14,15].

Tetraethylammonium hydroxide (TEAOH) is frequently used as an organic structure directing agent (OSDA) in the synthesis of Beta zeolites but a new method that does not require the use of OSDAs was discovered in 2008 [16]. Seeding crystals are used to direct the synthesis towards the formation of Beta zeolite. The resulting product has properties that are different from those of Beta from TEAOH synthesis, including a high aluminum content and relatively large crystal size [17]. In this contribution, the progress in the OSDA-free synthesis of Beta zeolite since its discovery is first briefly discussed. We then report on some of the catalytic properties of Beta zeolite from OSDA-free synthesis related to its specific characteristics, and on the possibility to post-synthetically modify the material. OSDA-free Beta before and after different modification treatments is compared to two commercially available Beta zeolites with different Si/Al ratios. Their performance is investigated in the alkylation of benzene with olefins of different chain length, in the acylation of aromatic ethers and in the hydroconversion of *n*-decane using bifunctional catalysts.

2. OSDA-free synthesis of Beta zeolite

The first synthesis of Beta zeolite used tetraethylammoniumhydroxide as OSDA. Typical synthetic Beta zeolites have Si/Al ratios in the range of 12-30 though purely siliceous Beta zeolites and aluminum-rich materials (Si/Al 5.2) have also been obtained using the same OSDA [11,18,19,20]. Various other synthesis strategies have been explored, resulting in a wide variety of zeolitic materials possessing the intergrown *BEA topology. For instance Beta zeolites containing other heteroatoms than Al – *e.g.* B, Ga, Ti, Sn, Zn or Zr - have been synthesized [21-27] and other OSDAs such as dibenzyldimethylammonium hydroxide, dicyclohexyldimethylammonium hydroxide or diaza-1,4-bicyclo[2.2.2] octane and methylamine have successfully been applied [28-30]. Crystal sizes can vary from the micrometer scale, typically for zeolites synthesized in presence of fluoride anions, to nanosized crystals [18,31]. The addition of seeds to the synthesis mixture has also been explored [25,32,33]. For a long time, however, the addition of an OSDA to the synthesis gel was required. The disadvantages of synthesis procedures using OSDAs are well known; they increase the cost of the zeolite production because of the increase in raw material cost and they necessitate high temperature calcination to remove the OSDA from the structure. In addition, the calcination step causes the emission of harmful gases. Of the five zeolite topologies that dominate the commercial zeolite catalyst production – FAU, MFI, *BEA, MOR and FER [4]– Beta was for a long time the only one that could not be obtained synthetically in the absence of an OSDA [1,34,35]. It should be noted, however, that the addition of OSDA can significantly speed up the crystallization process or may still be required to obtain alternative framework compositions for the above-mentioned topologies [28,36]. An indication that OSDAs are not strictly indispensable for Beta zeolite synthesis, appeared with the discovery of Tschernichite, the natural mineral analogue of Beta zeolite [37]. Tschernichite, which is a calcium aluminosilicate, shows the same intergrowth of polymorphs as synthetic zeolite Beta, but it has a high aluminum content (Si/Al 3.3) [38].

In 2008, Xiao and co-workers reported on the first synthesis of Beta zeolite in absence of OSDA [16]. A seeded synthesis approach was applied starting from an alkaline synthesis gel and the synthesis was completed after a hydrothermal treatment of less than a day. The addition of Beta seeds to the gel was essential as otherwise no Beta zeolite was obtained. Additional investigation of this type of Beta zeolite synthesis was performed by the group of Mintova [39] and they identified the obtained product as aluminum-rich (Si/Al 3.9 – 6.2). Variation of the type of inorganic cation showed that the use of Na^+ was more beneficial than use of Li^+ , K^+ or Ca^{2+}, even if Ca^{2+} is abundantly present in the natural Tschernichite. Nevertheless, only with Na^+, Beta zeolite could be obtained synthetically. The aluminum content in the synthesis gel was found to be a limiting factor for the crystallization and a reduced amount of seeds resulted in larger crystallite sizes. In a later report, Okubo's group successfully reused the Beta zeolites (Si/Al 5.4 – 6.6) from OSDA-free seeded synthesis as seed crystals, and named the obtained product "green Beta" as in this case, even the OSDA required for the seed crystals could be omitted [40]. In their synthesis conditions, mordenite was the thermodynamically more stable phase but the addition of Beta seeds kinetically favored the formation of Beta zeolites. The induction of Beta crystal growth on the seed surface was identified as an essential factor for obtaining OSDA-free Beta zeolite.

Further investigation into the crystallization mechanism was performed by the same group and resulted in a proposed synthesis mechanism in which the crystallization proceeds on the outer surface of the seeds; hence, the nucleation of Beta does not occur directly from the amorphous gel phase [41]. In order for Beta to grow, the seed crystals cannot be completely surrounded by the amorphous aluminosilicate phase. Dissolution of the initial gel during hydrothermal treatment brings the seed crystals to the interface of the aluminosilicate phase and the liquid phase where they can serve as a growth surface for new Beta crystals. This mechanism is in agreement with the one proposed by Xie *et al.* [17]. They found that the Beta seeds first partially dissolve in the alkaline synthesis medium, after which gradual crystal growth occurs according to a core-shell mechanism. A possible explanation for this switch from dissolution to growth could be the change in composition of the liquid phase surrounding the amorphous gel during hydrothermal treatment. This has also been suggested for template-free LTA synthesis [42].

The seeded synthesis approach in absence of OSDA can be extended to other framework types such as LEV, HEU, MTW, RTH and SZR [17,43,44,45,46]. Depending on the synthesis gel composition, the use of Beta seeds does not necessarily result in Beta zeolite as crystallization product. Using a different composition of the aluminosilicate synthesis gel than for the synthesis of OSDA-free Beta, Kamimura *et al.*[47] obtained MTW by addition of Beta seeds. Similarly, high-silica ferrierite could be obtained from the addition of RUB-37 seeds (CDO) to a synthesis gel that otherwise only yields small amounts of mordenite [48]. These interesting discoveries stimulated Okubo and co-workers to formulate a working hypothesis, based on common composite building units, for broadening the spectrum of zeolites that can be synthesized using OSDA-free, seeded synthesis [49].

Regarding the valorization of these materials from OSDA-free, seeded synthesis in catalysis, only few results have been published. Yokoi *et al.* [45] have tested RTH-type zeolites from OSDA-free synthesis in the methanol-to-olefins reaction (MTO) and obtained high selectivities to propene at high methanol conversions. OSDA-free ZSM-34, obtained from zeolite L seeds, was also used in MTO and higher selectivities to ethene and propene were obtained compared to

ZSM-5 [50]. The high aluminum content of MTW and Beta from OSDA-free seeded synthesis implies a high cation exchange capacity. This has been used to load these materials with silver and test their performance as antibacterial materials [51]. High cumene cracking activities have been obtained for aluminum-rich OSDA-free Beta and preliminary experiments showed that the material is active in benzene ethylation and anisole acylation [17, 52]. In the next sections, new results on the catalytic performance of OSDA-free Beta are presented.

3. Experimental

3.1 Catalysts

OSDA-free Beta zeolite (OF-Beta) was synthesized using an aluminosilicate gel with a molar ratio of 40 SiO_2 : 1 Al_2O_3 : 14.4 Na_2O : 1412 H_2O and calcined Beta zeolite seeds (Si/Al 11.6, 4.6% relative to the Si-source). In a typical synthesis procedure, the Al source (sodium aluminate, Al_2O_3 > 41.0%) was dissolved in distilled water. Sodium hydroxide (NaOH > 96%) and fumed silica were added after which the seeds were introduced. After stirring for 3 minutes, the synthesis gel was transferred into a Teflon lined autoclave and kept at 120°C for 120 h. The obtained powder was filtered, washed with distilled water and dried overnight at 80°C. To obtain the H^+-form, ion-exchange was performed in a 0.5 M NH_4NO_3 solution at 80°C for 24 h, followed by washing with distilled water and overnight drying at 70°C. The NH_4^+-exchanged zeolites were calcined in air at 450°C for 5 h (heating rate 1°C/min).

Steam dealumination of OF-Beta was performed by repeated ion exchange with NH_4NO_3 followed by steam treatment. The sample was ion exchanged with a 4 M NH_4NO_3 solution at reflux, hydrated and heated in a covered vessel to 600°C (heating rate 1°C/min) for 2 h. Ion-exchange and steam treatment were repeated three times. The obtained sample was labeled OF-Beta-ST.

Part of OF-Beta-ST was further dealuminated by acid leaching with an aqueous HNO_3 solution for 3 h at 80°C, using 2 g OF-Beta-ST per 100 ml HNO_3 solution. After the acid treatment, samples were washed with distilled water and dried at 80°C. The HNO_3 concentrations used were 0.1 M, 0.5 M and 6.0 M resulting in the respective samples OF-Beta-ST-0.1, OF-Beta-ST-0.5 and OF-Beta-ST-6.0.

Commercial Beta zeolites Beta-1 (CP811 BL-25, PQ Corp., obtained in the H^+-form) and Beta-2 (CP814C, Zeolyst, obtained in the NH_4^+-form) were used as reference materials from templated synthesis.

3.2 Catalyst characterization

Powder X-ray diffraction patterns (PXRD) were collected on a STOE Stadi MP diffractometer in Debeye-Scherrer geometry with Cu-$K\alpha_1$ radiation, a linear position sensitive detector (PSD) (6 °2θ window) and the sample in a capillary sample holder. To determine the crystal size and morphology, scanning electron microscopy (SEM) images were taken using a Philips XL30 FEG. Textural properties were analyzed based on N_2 adsorption isotherms, determined by physisorption at 77 K on a Coulter Omnisorp 100 CX. Prior to measurement, the samples were outgassed under vacuum at 200°C overnight. Bulk elemental analysis was performed on a Varian Vista-PRO inductively coupled plasma optical emission spectrometer (ICP-OES).

FTIR spectrometry was used to investigate the hydroxyl stretching region and to determine the Lewis and Brønsted acidity using pyridine as probe molecule. IR spectra of self-supporting

wafers of the zeolite samples (thickness 10-15 cm^2/g) were measured on a Nicolet 6700 FT-IR spectrometer with DTGS detector (128 scans, 2 cm^{-1} resolution). Reference spectra were recorded at 150°C after heating under vacuum to 450°C for 1 h. Acidity was probed using pyridine adsorption. Pyridine (25 mbar) was allowed to adsorb at 50°C and after saturation, the samples were evacuated for 30 min to remove the physisorbed pyridine before reheating (4°C/min) to 150°C and recording IR spectra of the samples containing chemisorbed pyridine. The number of acid sites was evaluated from the integral intensities of the absorption bands corresponding to pyridine adsorbed on Lewis (1450 cm^{-1}) and Brønsted acid sites (1545 cm^{-1}) using the molar extinction coefficients of Emeis [53].

The number of acid sites on the samples was also quantified using temperature programmed desorption of ammonia (NH_3 TPD) measured on a Micromeritics AutoChem II 2920 automated chemisorption analysis unit with a thermal conductivity detector (TCD) under helium flow. An on-line mass spectroscopy (MS) system for continuous analysis of the desorbed species was used to confirm that the TCD signal corresponded to ammonia desorption. In all samples, two desorption peaks were observed and the amount of NH_3 desorbing at each peak was obtained via deconvolution.

3.3 Catalytic reactions

Alkylation: Alkylation of benzene (Sigma-Aldrich, 99.7%) with ethene (Air Liquide, 99.95%) or propene (Air Liquide, 99.5%) was performed in a Parr reactor (capacity 100 mL) at 150°C. Prior to reaction, the zeolite catalysts (calcined, H^+-form) were activated at 200°C in an oven for 14 h. The reactor was loaded under N_2 atmosphere with 40 mL benzene and 62.5 mg dried catalyst. The reactor was flushed and subsequently saturated with 5 bar ethene for 30 min (molar ratio benzene : ethene 8) or with 1 bar propene for 60 min (molar ratio benzene : propene 6), pressurized with 50 bar N_2 and heated to 150°C. The reaction mixture was stirred at 1250 rpm.

Alkylation of 1-dodecene (Acros, 93-95%) was performed in a 60 mL reactor that was loaded under N_2 atmosphere with 100 mg dried catalyst, 8.4 mL benzene, 21.1 mL *n*-decane (Acros, 99%) and 2.4 mL 1-dodecene (molar ratio benzene : 1-dodecene 20), pressurized with 30 bar N_2 and heated to 120°C with stirring speed 1250 rpm.

Acylation: Acylation of anisole (Acros, 98%) with acetic anhydride (VWR, 98%) was performed at 90°C in glass crimp cap reactor vials loaded under N_2 atmosphere with 100 mg dried catalyst (H^+-form), 5.3 g anisole and 1 g acetic anhydride (molar ratio anisole : acetic anhydride 5). The reactor vials were placed in a heated copper block and stirred at 500 rpm.

Acylation of 2-methoxynaphthalene (Acros, 98%) with acetic anhydride was performed at 110°C in glass crimp cap reactor vials loaded under N_2 atmosphere with 240 mg dried catalyst (H^+-form), 6 mmol 2-methoxynaphthalene, 3 mmol acetic anhydride and 4.5 mL chlorobenzene. The reactor vials were placed in a heated copper block and stirred at 500 rpm.

During the acylation and alkylation reactions, samples were taken periodically and analyzed on a Shimadzu GC equipped with a 60 m CP-Sil-5CB column and FID detector. Peak identification was performed using authentic samples and GC/MS.

Hydroconversion: For the hydroconversion of *n*-decane the zeolite samples were transformed into bifunctional catalysts. First the samples were transformed into the NH_4^+-form by three ion exchange steps with 0.5M NH_4NO_3 at 80°C for 24 h followed by washing with distilled water. After drying at 70°C, Pt (0.5 wt.%) was loaded onto the catalyst via competitive ion exchange as $Pt(NH_3)_4^{2+}$ using an aqueous solution of $Pt(NH_3)_4Cl_2$. The samples were compressed and the wafers were broken up and sieved to obtain a fraction of 125-250 µm particles. 50 mg of catalyst pellets was loaded into a quartz reactor tube (internal diameter 2 mm).

Before reaction, the Pt containing samples were first treated with an O_2-flow of 1.9 ml/min at 400°C for the oxidation followed by a H_2-flow of 3.8 ml/min at 400°C for the reduction of platinum. An intermediate cooling step was carried out under He atmosphere. The *n*-decane hydroconversion experiments were performed at temperatures ranging from 170°C to 280°C, under 4.5 bar H_2 pressure, at a H_2 : decane molar ratio of 375 using a fixed space time of 2522 kg s/mol and stepwise temperature increase. Samples from the reactor outlet were injected into a capillary GC equipped with a 25 m CP-Sil-5 column. Conversion values were calculated from the integrated area of the *n*-decane peak before and during reaction. Yields of isomerization and cracking products were determined from the respective chromatograms.

4. Results

4.1 Characterization

Elemental analysis and textural characterization data of selected samples are shown in Table 1. OF-Beta has a low Si/Al ratio typical for Beta zeolites from OSDA-free synthesis [17,39,40]. Using steam dealumination (OF-Beta-ST), the aluminum content of OF-Beta can be significantly reduced while simultaneously increasing the mesopore volume. Further dealumination via acid leaching leads to gradually increasing Si/Al ratios. The PXRD patterns (Fig. 1) of the OSDA-free Beta zeolites show sharp peaks in the low angle region compared to the commercial Beta zeolites Beta-1 and Beta-2. The sharp peak at 22.1° 2θ is consistent with other reports on aluminum-rich zeolite Beta and its natural mineral analogue Tschernichite. Its position at lower angles compared to the 22.5-22.6° 2θ of the commercial Beta zeolites has been related to the high framework aluminum content [17,38,39]. Upon dealumination, the Bragg reflections show more resemblance to those of the more Si-rich commercial Beta zeolites.

Table 1: Elemental composition and textural properties.

Figure 1: XRD patterns for BEA-1 (a), BEA-2 (b), OF-BEA (c), OF-BEA-ST (d), OF-BEA-ST-0.1 (e), OF-BEA-ST-0.5 (f) and OF-BEA-ST-6.0 (g).

SEM images (Fig.2) of OF-Beta show intergrown crystals with a truncated octahedral morphology and well-defined surfaces. The crystallites of OF-Beta measure up to 500-800 nm, which is clearly much larger than those of the commercial Beta zeolites used as reference materials in this study. The latter consist of aggregates of small particles in which no well-defined morphology can be recognized. Steam dealumination of OF-Beta degrades part of the crystals but the truncated octahedral morphology can still be distinguished.

Figure 2: SEM images of Beta-1 (a), Beta-2 (b), OF-Beta (c) and OF-Beta-ST (d).

The infrared hydroxyl stretching region of the different zeolite samples is shown in Fig. 3. It is clear that OF-Beta contains a large amount of bridging hydroxyl groups (3607 cm^{-1}) which can be related to its high aluminum content. It also contains a moderate absorption band at 3660 cm^{-1} which could correspond to hydroxylated monomeric or polymeric extra-framework aluminum species [54,55]. The absorption bands corresponding to non-acidic hydroxyl groups at the outer surface (3742 cm^{-1}) and at defect sides inside the crystals (3735 cm^{-1}) [54,55] are much less pronounced for OF-Beta than for the commercial Beta zeolites Beta-1 and Beta-2. This is consistent with the larger crystal size of OF-Beta and also implies that OF-Beta contains less internal defects and is more crystalline – a feature of Beta zeolites from seeded, OSDA-free synthesis that has been suggested in previous reports based on the sharpness of some reflections in PXRD, the high micropore volume and micropore surface area compared to Beta zeolites from templated synthesis [17,39,40]. After steam dealumination, the intensity of the bridging hydroxyl groups diminishes whereas the absorption bands corresponding to defect sites and external hydroxyl groups become more prominent. Using adsorption of pyridine as a probe molecule, the relative contributions of Brønsted and Lewis acid sites were determined (Table 2). Fig. 4 shows the difference spectra after adsorption of pyridine; it is evident that OF-Beta contains a larger amount of Brønsted acid sites compared to the commercial Beta zeolites Beta-1 and Beta-2. Consistent with the diminished bridging hydroxyl vibration, the amount of pyridine adsorbed also decreases after steam dealumination.

Figure 3: Infrared hydroxyl stretching region of BEA-1 (a), BEA-2 (b), OF-BEA (c) and OF-BEA-ST (d) , normalized to 10 mg/cm^2.

Figure 4: Difference IR spectra of adsorbed pyridine on Beta-1 (a), Beta-2 (b), OF-Beta (c) and OF-Beta-ST (d), normalized to 10 mg/cm^2. The absorption bands at 1450 cm^{-1} and 1545 cm^{-1} correspond to pyridine adsorbed on Lewis resp. Brønsted acid sites.

Acidity of the samples was also characterized using temperature programmed desorption of ammonia (Table 2). OF-Beta does not only contain a large amount of acid sites, but judging from the temperature at which the NH_3 desorbs, the acid sites seem to be remarkably strong. Upon steam dealumination, the amount of acid sites of OF-Beta is reduced to less than one third.

Table 2: Acidic properties determined with NH_3 TPD and FTIR using pyridine as probe molecule

4.2 Alkylation

The catalytic activity of OF-Beta and the derived materials was investigated in the alkylation of benzene with olefins of different chain length. In a first alkylation experiment, ethene was used as alkylating agent, using an excess of the aromatic reactant as is usual in industrial alkylation. Fig. 5 shows the activity and selectivity towards the monoalkylated product for the different tested materials. Remarkably, OF-Beta shows the highest activity in this reaction. Most of the activity is preserved after the steam dealumination treatment, but the subsequent acid leaching treatment with HNO_3 leads to a continuous drop in activity with increasing HNO_3 concentration. For instance, OF-Beta-ST-6.0 is almost completely inactive in this reaction. OF-Beta also shows a remarkably higher selectivity towards the monoalkylated ethylbenzene than commercial Beta zeolites Beta-1 and Beta-2. Besides a high activity and selectivity, the OF-Beta sample is also least sensitive to coke formation; coke, as evaluated in TGA measurements, amounted to only 5 wt.% for a used OF-Beta sample, against 8-9 wt. % for the used commercial samples Beta-1 and

Beta-2. Coke formation in these reactions is typically due to multiple alkylation, suggesting that the desorption of the primary ethylbenzene product is easier in the OF-Beta sample than in other, more Si-rich catalysts. The steam dealumination treatment on the other hand does not only lead to a reduced activity but also to a lower selectivity at higher conversions. Given their low activity, the selectivity for OF-Beta-ST-0.1/0.5/6.0 is not shown as it cannot be compared at similar conversions.

Figure 5: Benzene conversion (left) in the liquid phase alkylation of benzene with ethene (benzene : ethene 8, reaction temperature 150°C) and selectivity referred to ethene to the monoalkylated ethylbenzene for BEA-1 (▲), BEA-2 (◆), OF-BEA (■), OF-BEA-ST (●), OF-BEA-ST-0.1 (△), OF-BEA-ST-0.5 (◇) and OF-BEA-ST-6.0 (□).

The promising activity and selectivity of OF-Beta in the alkylation with ethene encouraged us to investigate its performance in alkylations of benzene with more reactive, longer chain olefins such as propene and 1-dodecene. Conversions in these reactions are shown in Fig. 6. In contrast to the ethylation reaction, much lower conversions are obtained with OF-Beta as catalyst than with the commercial Beta zeolites in the alkylations with both propene and 1-dodecene. The limited further increase in conversion after the first five hours of reaction indicates that deactivation could play a significant role. The steam dealumination treatment, which introduces an increase in mesopore volume in OF-Beta, has a positive influence on the activity and stability of OF-Beta in the alkylation with propene. In the alkylation with 1-dodecene however, all Beta zeolites obtained through OSDA-free synthesis suffered from fast deactivation and much lower conversions were obtained than with commercial zeolites Beta-1 and Beta-2.

Figure 6: Benzene conversion in the liquid phase alkylation of benzene with propene (left, benzene : propene 6, reaction temperature 150°C) and dodecene conversion in the alkylation of benzene with 1-dodecene (right, benzene : 1-dodecene 8.6, reaction temperature 120°C) for BEA-1 (▲), BEA-2 (◆), OF-BEA (■), OF-BEA-ST (●).

4.3 Acylation

The acylation activity of OF-Beta can be strongly enhanced by post-synthesis dealumination treatment. Fig. 7 shows the conversion of acetic anhydride in the acylation of anisole and of 2-methoxynaphthalene. The poor conversion with OF-Beta in both acylation reactions again seems to suggest strong deactivation. Steam dealumination increases the activity of OF-Beta up to an activity level that is comparable to that of the commercial Beta zeolites Beta-1 and Beta-2. In the anisole acylation, acid leaching with 0.5 M HNO_3 leads to an even slightly more active catalyst, but treatment with 6M HNO_3 is no longer beneficial for the activity. The selectivity towards *p*-methoxyacetophenone was higher than 98% for all catalysts.

The positive effect of acid leaching on the activity of OF-Beta-ST in the anisole acylation, does not extend to the 2-methoxynaphthalene acylation. Acid treatment results in even lower conversions than for the original OF-Beta. The main reaction products observed in the acylation of 2-methoxynaphthalene are 1-acetyl-2-methoxynaphthalene (1,2-AMN) and 2-acetyl-6-methoxynaphthalene (Fig. 8) with a combined selectivity to the other side-products (other acetylmethoxynaphthalene isomers and diacetylated products) of less than 10% for all catalysts. Except for OF-Beta, all catalysts show an increase in selectivity for 2,6-AMN and a decrease for

1,2-AMN with increasing conversion. The selectivity of OF-Beta-ST for both 1,2-AMN and 2,6-AMN lies in between that of commercial Beta-1 and Beta-2.

Figure 7: Acetic anhydride conversion in the acylation of anisole (left, molar ratio anisole / acetic anhydride 5) and 2-methoxynaphthalene (right, molar ratio 2-methoxynaphthalene / acetic anhydride 2) for Beta-1 (▲), Beta-2 (◆), OF-Beta (■), OF-Beta-ST (●), OF-Beta-ST-0.1 (△), OF-Beta-ST-0.5 (◇) and OF-Beta-ST-6.0 (□).

Figure 8: Selectivity to 1-acetyl-2-methoxynaphthalene (left) and 2-acetyl-6-methoxynaphthalene (right) as function of acetic anhydride conversion in the acylation of 2-methoxynaphthalene for Beta-1 (▲), Beta-2 (◆), OF-Beta (■), OF-Beta-ST (●), OF-Beta-ST-0.1 (△), OF-Beta-ST-0.5 (◇) and OF-Beta-ST-6.0 (□).

4.4 Hydroconversion

The Beta zeolite samples were transformed into bifunctional catalysts by loading with 0.5 wt.% Pt and tested in the hydroconversion of *n*-decane using a constant space time (Fig. 9). OF-Beta shows full conversion of *n*-decane at temperatures as low as 190°C. In addition, its isomerization yields at lower conversion are rather low, which can be ascribed to an imbalance between the Pt dehydrogenation/hydrogenation sites and the high amount of acid isomerization sites related to the framework aluminum. In comparison, commercial Beta-1 with the same Pt loading but lower aluminum content reaches an isomerization yield of 13.0 % at 73.4 % conversion whereas OF-Beta yields only 1.5 % of isomerization products at 79.5 % conversion. The primary cracking products comprise the expected range of linear or branched hydrocarbons, with carbon numbers between C2 and C8. As the hydroconversions were performed under hydrogen using bifunctional catalysts, olefins are quickly rehydrogenated to alkanes, which effectively suppresses any formation of deactivating coke. The steam dealuminated OF-Beta-ST is only slightly less active than its parent material. Further dealumination by acid leaching leads to a stronger decrease in activity, as can be seen from the higher temperatures required to obtain the same level of conversion. However, the gradual dealumination combined with constant Pt loading results in higher isomerization yields (Fig. 10).

Figure 9: Catalytic results from the n-decane hydroconversion: n-decane conversion (◆), yield of isomerization products (■) and yield of cracking products (▲) for Beta-1 (a), OF-Beta (b), OF-Beta-ST (c), OF-Beta-ST-0.1 (d), OF-Beta-ST-0.5 and OF-Beta-ST-6.0 (e).

Figure 10: Yield of isomerized products as function of n-decane conversion for Beta-1 (▲), OF-Beta (■), OF-Beta-ST (●), OF-Beta-ST-0.1 (△), OF-Beta-ST-0.5 (◇) and OF-Beta-ST-6.0 (□).

5. Discussion

The investigated probe reactions require different key characteristics of zeolite catalysts for optimal performance. For instance in alkylation reactions with the rather unreactive ethene, the presence of strong acid sites is necessary to activate ethene [56]. In acetylation reactions of aromatic ethers, framework polarity of the zeolite catalyst is an important factor to avoid deactivation caused by the competitive adsorption of the polar products [57,58] and in the hydroconversion of alkanes, the balance between the acid sites and the hydrogenation/dehydrogenation sites is vital to obtain high isomerization yields [59].

The influence of the aluminum content of zeolite Beta on the liquid phase alkylation of benzene with short-chain olefins like ethene or propene was investigated by Bellussi *et al.* [8]. They found that higher Al-contents resulted in an increase not only of the activity, but also of the selectivity for alkylation *vs.* side reactions like olefin oligomerization. However, the range of Al-contents in which they investigated this reaction (Si/Al 14-112) was limited by the amount of aluminum that could be incorporated via templated synthesis. The OSDA-free synthesis of Beta zeolites has widened this range to even higher aluminum contents. For the alkylation of benzene with ethene, this improvement in activity and selectivity seems to continue when Beta zeolites from OSDA-free synthesis are used. This is quite remarkable because the activation of ethene requires strong acidity. For high aluminum contents, a lower acid site strength would be expected [2,60]. The high activity, as proven by the results of Fig. 5, is, in addition to the NH_3-TPD and FTIR results, another indication that OF-Beta indeed not only contains a large number of active sites, but that these sites still possess very strong Brønsted acidity. Moreover, when the ethylbenzene selectivity is plotted *vs*. the benzene conversion (Fig. 5), the OF-Beta produces systematically more of the monoalkylation product than the templated zeolites. One possible explanation for the high selectivity towards ethylbenzene could be the high framework polarity of OF-Beta, in comparison with the templated Beta zeolites. For OF-Beta, this framework polarity would increase the adsorption preference for benzene over ethylbenzene, which would relatively favor alkylation of benzene over a second alkylation of ethylbenzene to diethylbenzene. Nevertheless, besides the effect of the elemental composition, additional effects of crystal size and texture cannot be excluded.

Bellussi *et al.* [8] also reported an increase in performance with increasing aluminum content of Beta zeolite in the alkylation with propene. However, in the alkylation with propene, this trend does not continue when using OF-Beta with its very high Al contents. Even though propene and ethene both can be considered as 'light olefins', their reactivities are markedly different and propene oligomerization is a much more important side reaction [61,62]. The propene oligomers themselves can also lead to larger and heavier by-products that can remain adsorbed on the zeolite surface or that block the access to the pores. Given the relatively large crystal size of OF-Beta, the material is more susceptible to deactivation through pore blocking [63]. The alkylation of benzene with long-chain olefins such as 1-dodecene is known to be even more sensitive to deactivation through pore blocking because of the various bulky by-products that can be formed through double bond migration, dimerization and alkylation with isomerized olefins [15]. Post-synthesis modifications to increase accessibility of sites and stability are often performed; especially introducing mesoporosity in mordenite has proven successful [64-66]. The steam dealumination that increases the mesopore volume of OF-Beta has a stabilizing effect in the alkylation with propene, and the dealuminated sample performs much better than the as-synthesized Al-rich sample (Fig. 6). However, this modification does not suffice to prevent deactivation when using longer olefins like 1-dodecene (Fig. 6). Other modifications, such as an even more thorough dealumination or a modification of the synthesis procedure to obtain smaller crystals, could be helpful in increasing accessibility of the sites and preventing deactivation. It should be noted however that smaller crystal sizes do not necessarily lead to better deactivation resistance. In the alkylation of toluene with long-chain olefins, Da *et al.* [15] noticed that even small Beta crystallites can suffer from fast deactivation compared to a Y-type zeolite of similar acidity. This was attributed to the slow desorption of the reaction products from the narrow pores.

In the acylation of anisole, framework hydrophobicity plays an important role because the products are more polar and heavier than the reactants and tend to remain preferentially adsorbed on the zeolite framework. Especially on hydrophilic frameworks, this type of product inhibition is an important cause of deactivation [57,58,67]. Derouane *et al.* [58] investigated the influence of the zeolite catalyst Si/Al ratio on the activity and deactivation of Beta zeolite catalysts in acylations. At high aluminum contents (Si/Al 12.5), deactivation by product inhibition was the cause of low yields. Dealumination improved the activity but at higher Si/Al ratios (Si/Al 93.3), again, lower yields were obtained. This was attributed to the small number of acid sites. In our experiments, similar observations can be made. The framework polarity of OF-Beta causes rapid deactivation through product inhibition. Steam dealumination leads to a (bulk) Si/Al ratio comparable to that of the commercial Beta zeolites used and the activity increases accordingly. Further dealumination through acid leaching eventually results in a decrease in activity when too high concentrations of HNO_3 are used (OF-Beta-6.0). This is probably caused by the lower concentration of acid sites. Beers *et al.* [68] also investigated the influence of dealumination of Beta zeolites on the acylation of anisole, using octanoic acid as acylating agent. They proposed that the increase in activity resulted from increased accessibility and this may also contribute to the activity increase of OF-Beta-ST compared to the parent OF-Beta.

The acylation of 2-methoxynaphthalene occurs preferentially on two positions. Kinetically, the formation of 1,2-AMN is preferred over the thermodynamically more stable 2,6-AMN. Both products can be formed via direct acylation but consecutive reaction can transform 1,2-AMN into the smaller 2,6-AMN or back to 2-methoxynaphthalene through deacylation [10,69]. Inside the pores of Beta, steric hindrance leads to a preferential formation of 2,6-AMN but on the outer surface, 1,2-AMN is mainly formed. Though increased crystal size has been reported to be beneficial for 2,6-AMN selectivity [10], this is not observed for OF-Beta. Its low activity can again be attributed to the high framework polarity leading to fast deactivation. Comparison is difficult considering its low activity, but the high selectivity to 1,2-AMN indicates that the access to the inner surface is rapidly blocked and the subsequent conversion proceeds mainly on the outer surface. The steam dealumination again leads to an activity improvement with selectivities in between those of the two commercial Beta catalysts. Subsequent acid leaching leads to serious reductions in activity.

Hydroconversion of alkanes over bifunctional catalysts uses the metallic sites for dehydrogenation and hydrogenation; the acid sites catalyze isomerization and cracking steps. To obtain high isomerization yields, the distance between the acid sites and metal sites should be small enough to hydrogenate the isoalkenes before further reaction on acid site leads to cracking. On an ideal hydroisomerization catalyst, the olefinic intermediates are transformed only once on an acid site before being hydrogenated. Alvarez *et al.* [59] investigated the balance of the hydrogenating and acid functions in the *n*-decane hydroconversion to find the ideal PtHY hydroisomerization catalyst. Beta-1, OF-Beta and OF-Beta-ST already reach a very high conversion of *n*-decane in the investigated temperature window (Fig. 9 a,b,c) and high cracking yields are to be expected. These catalysts were also the most active in the demanding ethylation reaction. Clearly, they contain such a high concentration of active sites that it is impossible to balance them with the fixed amount of Pt used, especially if large crystallites are used. The acid treatment after steam dealumination leads to a decrease in the number of acid sites, resulting in an improved balance of hydrogenation and acid sites and much higher isomerization yields.

6. Conclusion

In the various reactions that were probed, Beta zeolites from OSDA-free synthesis have different properties than the usual commercial Beta zeolites. Part of the differences can be explained by the higher aluminum content and different crystal size. The high aluminum content leads to a large number of acid sites of considerable strength resulting in an active ethylation catalyst even at 150°C.

The large crystal size of OSDA-free Beta zeolites makes them sensitive to deactivation through pore blocking. In alkylation reactions with propene and 1-dodecene, this resulted in low activities. An appropriate dealumination treatment can improve the accessibility and delay the deactivation. The high aluminum content also leads to a high framework polarity which is a cause for fast deactivation in acylation reactions. This can be prevented by dealumination where an activity optimum is obtained between framework polarity and acid site concentration.

The high amount of strong acid sites also leads to a high yield of cracked products in the n-decane hydroconversion at very low temperatures. Clearly more Pt should be added to improve the balance between the acid sites and (de)hydrogenation sites. A reduction of the amount of acid sites by dealumination at constant Pt loadings resulted in higher isomerization yields.

Acknowledgements

This work was performed under the framework of the INCOE projected, coordinated by BASF. T.D.B. acknowledges F.W.O.-Vlaanderen (Research Foundation - Flanders) for a doctoral fellowship.

References

[1] D.W. Breck, Zeolite Molecular Sieves: Structure, Chemistry and Use, Wiley, New York, 1974, p 771.
[2] J. Weitkamp, Solid State Ionics 131 (2000) 175.
[3] http://www.iza-structure.org (24.02.2013).
[4] S. Zones, Micropor. Mesopor. Mater. 144 (2011) 1.
[5] R.A. Innes, S.I. Zones, G.J. Nacamuli, US Patent 4891450 (1990), to Chevron USA Inc.
[6] F. Cavani, V. Arrigoni, G. Bellussi, EP 0432814 A1 (1991), to Enirecerche, EniChem.
[7] C. Perego, P. Ingallina, Green Chem. 6 (2004) 274.
[8] G. Bellussi, G. Pazzuconi, C. Perego, G. Girotti, G. Terzoni, J. Catal. 157 (1995) 227.
[9] M. Spagnol, L. Gilbert, H. Guillot, P.-J. Tirel, WO Patent WO 97/48665 (1997), to Rhone-Poulenc Chimie, France.
[10] P. Andy, J. Garcia-Martinez, G. Lee, H. Gonzalez, C. Jones, M. Davis, J. Catal. 192 (2000) 215.
[11] R.L. Wadlinger, G. T. Kerr, E. J. Rosinski, US Patent 3 308 069 (1967), to Mobil Oil Corporation.
[12] J. Newsam, M. Treacy, W. Koetsier, C. De Gruyter, Proc. R. Soc. London, Ser. A (1988) 375
[13] J. Higgins, R.B. LaPierre, J. Schlenker, A. Rohrman, J. Wood, G. Kerr, W. Rohrbaugh, Zeolites 8 (1988) 446.
[14] J.A. Martens, M. Tielen, P.A. Jacobs, J. Weitkamp, Zeolites 4 (1984) 98.
[15] Z. Da, Z. Han, P. Magnoux, M. Guisnet, Appl. Catal., A 219 (2001) 45.
[16] B. Xie, J. Song, L. Ren, Y. Ji, J. Li, F.-S. Xiao, Chem. Mater. 20 (2008) 4533.

[17] B. Xie, H. Zhang, C. Yang, S. Liu, L. Ren, L. Zhang, X. Meng, B. Yilmaz, U. Mueller, F.-S. Xiao, Chem. Commun. 47 (2011) 3945.
[18] S. Mintova, V. Valtchev, T. Onfroy, C. Marichal, H. Knözinger, T. Bein, Microporous Mesoporous Mater. 90 (2006) 237.
[19] M.A. Camblor, A. Corma, S. Valencia, Chem. Commun. (1996) 2365.
[20] R.B. Borade, A. Clearfield, Microporous Mater. 5 (1996) 289.
[21] B. Marler, R. Böhme, H. Gies; R. von Ballmoos, J.B. Higgins, M.J. Treacy (Eds.), Proceedings of the Ninth International Conference on Zeolites, Butterworth-Heinemann, London (1993), p. 425.
[22] K. Reddy, M. Eapen, P. Joshi, S. Mirajkar, V. Shiralkar, J. Inclusion Phenom. Macrocyclic Chem. 20 (1994) 197.
[23] M.A. Camblor, A. Corma, A. Martínez, J. Pérez-Pariente, J. Chem. Soc., Chem. Commun. (1992) 589.
[24] T. Blasco, M.A. Camblor, A. Corma, P. Esteve, A. Martínez, C. Prieto, S. Valencia, Chem. Commun. (1996) 2367.
[25] A. Corma, L. T. Nemeth, M. Renz, S. Valencia, Nature 412 (2001) 423.
[26] T. Takewaki, L.W. Beck, M.E. Davis, Top. Catal. 9 (1999) 35.
[27] Y. Zhu, G. Chuah, S. Jaenicke, Chem. Commun. (2003) 2734.
[28] J.C. van der Waal, M.S. Rigutto, H. van Bekkum, J. Chem. Soc., Chem. Commun. (1994) 1241.
[29] J. van der Waal, P. Kooyman, J. Jansen, H. van Bekkum, Micropor. Mesopor. Mater. 25 (1998) 43.
[30] P. Caullet, J. Hazm, J. Guth, J. Joly, J. Lynch, F. Raatz, Zeolites 12 (1992) 240.
[31] M.A. Camblor, A. Corma, S. Valencia, J. Mater. Chem. 8 (1998) 2137.
[32] T. Blasco, M.A. Camblor, A. Corma, P. Esteve, J.M. Guil, A. Martinez, J.A. Perdigon-Melon, S. Valencia, J. Phys. Chem. B 102 (1998) 75.
[33] T.R. Cannan, R.J. Hinchey, US Patent 5 139 759 (1992), to UOP.
[34] V. Shiralkar, A. Clearfield, Zeolites 9 (1989) 363.
[35] D.B. Hawkins, Mater. Res. Bull. 2 (1967) 951.
[36] P.K. Dutta, K.M. Rao, J.Y. Park, Langmuir 8 (1992) 722.
[37] J.V. Smith, J.J. Pluth, R.C. Boggs, D.G. Howard, J. Chem. Soc., Chem. Commun. (1991) 363.
[38] R. Szostak, K.P. Lillerud, M. Stocker, J. Catal. 148 (1994) 91.
[39] G. Majano, L. Delmotte, V. Valtchev, S. Mintova, Chem. Mater. 21 (2009) 4184.
[40] Y. Kamimura, W. Chaikittisilp, K. Itabashi, A. Shimojima, T. Okubo, Chem.–Asian J. 5 (2010) 2182.
[41] Y. Kamimura, S. Tanahashi, K. Itabashi, A. Sugawara, T. Wakihara, A. Shimojima, T. Okubo, J. Phys. Chem. C 115 (2011) 744.
[42] L. Itani, Y. Liu, W. Zhang, K. Bozhilov, L. Delmotte, V. Valtchev, J. Am. Chem. Soc. 131 (2009) 10127.
[43] K. Iyoki, Y. Kamimura, K. Itabashi, A. Shimojima, T. Okubo, Chem. Lett. 39 (2010) 730.
[44] Y. Kamimura, K. Itabashi, T. Okubo, Micropor. Mesopor. Mater. 147 (2012) 149.
[45] T. Yokoi, M. Yoshioka, H. Imai, T. Tatsumi, Angew. Chem. 121 (2009) 10068.
[46] W. Zhang, Y. Wu, J. Gu, H. Zhou, J. Wang, Mater. Res. Bull. 46 (2011) 1451.
[47] Y. Kamimura, K. Iyoki, S.P. Elangovan, K. Itabashi, A. Shimojima, T. Okubo, Micropor. Mesopor. Mater. 163 (2012) 282.

[48] H. Zhang, Q. Guo, L. Ren, C. Yang, L. Zhu, X. Meng, C. Li, F.-S. Xiao, J. Mater. Chem. 21 (2011) 9494.
[49] K. Itabashi, Y. Kamimura, K. Iyoki, A. Shimojima, T. Okubo, J. Am. Chem. Soc. 134 (2012) 11542.
[50] L. Zhang, C. Yang, X. Meng, B. Xie, L. Wang, L. Ren, S. Ma, F.-S. Xiao, Chem. Mater. 22 (2010) 3099.
[51] P. Saint-Cricq, Y. Kamimura, K. Itabashi, A. Sugawara-Narutaki, A. Shimojima, T. Okubo, Eur. J. Inorg. Chem. 2012 (2012) 3398.
[52] B. Yilmaz, U. Mueller, M. Feyen, S. Maurer, X. Meng, F.-S. Xiao, W. Zhang, H. Imai, T. Yokoi, T. Tatsumi, H. Gies, T. De Baerdemaeker and D. E. De Vos, Catal. Sci. Technol. (2013) DOI: 10.1039/C3CY00073G, in press.
[53] C. Emeis, J. Catal. 141 (1993) 347.
[54] A. Simon-Masseron, J. Marques, J. Lopes, F.R. Ribeiro, I. Gener, M. Guisnet, Appl. Catal., A 316 (2007) 75.
[55] I. Kiricsi, C. Flego, G. Pazzuconi, W.O.J. Parker, R. Millini, C. Perego, G. Bellussi, J. Phys. Chem. 98 (1994) 4627.
[56] X. Sun, Q. Wang, L. Xu, S. Liu, Catal. Lett. 94 (2004) 75.
[57] E. Derouane, C. Dillon, D. Bethell, S. Derouane-Abd Hamid, J. Catal. 187 (1999) 209.
[58] E. Derouane, G. Crehan, C. Dillon, D. Bethell, H. He, S. Derouane-Abd Hamid, J. Catal. 194 (2000) 410.
[59] F. Alvarez, F. Ribeiro, G. Perot, C. Thomazeau, M. Guisnet, J. Catal. 162 (1996) 179.
[60] J.A. Lercher, A. Jentys, in: C. Martínez, J. Pérez-Pariente (Eds), Zeolites and ordered porous solids: fundamentals and applications, Editorial Universitat Politècnica de València, Valencia, 2011, p. 371.
[61] T.F. Degnan, C.M. Smith, C.R. Venkat, Appl. Catal., A 221 (2001) 283.
[62] C. Perego, P. Ingallina, Catal. Today 73 (2002) 3.
[63] M. Guisnet, L. Costa, F.R. Ribeiro, J. Mol. Catal. A: Chem. 305 (2009) 69.
[64] P. Magnoux, A. Mourran, S. Bernard, M. Guisnet, Stud. Surf. Sci. Catal. 108 (1997) 107.
[65] M. Boveri, C. Márquez-Álvarez, M.Á. Laborde, E. Sastre, Catal. Today 114 (2006) 217.
[66] J.-S. Lin, J.-J. Wang, J. Wang, I. Wang, R.J. Balasamy, A. Aitani, S. Al-Khattaf, T.-C. Tsai, J. Catal. 300 (2013) 81.
[67] D. Rohan, C. Canaff, E. Fromentin, M. Guisnet, J. Catal. 177 (1998) 296.
[68] A. Beers, J. van Bokhoven, K. De Lathouder, F. Kapteijn, J. Moulijn, J. Catal. 218 (2003) 239.
[69] P. Botella, A. Corma, M. Navarro, F. Rey, G. Sastre, J. Catal. 217 (2003) 406.

List of figures

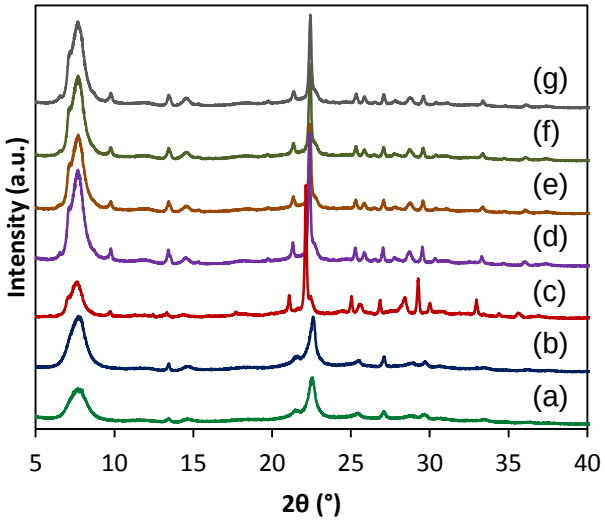

Figure 1: XRD patterns for Beta-1 (a), Beta-2 (b), OF-Beta (c), OF-Beta-ST (d), OF-Beta-ST-0.1 (e), OF-Beta-ST-0.5 (f) and OF-Beta-ST-6.0 (g).

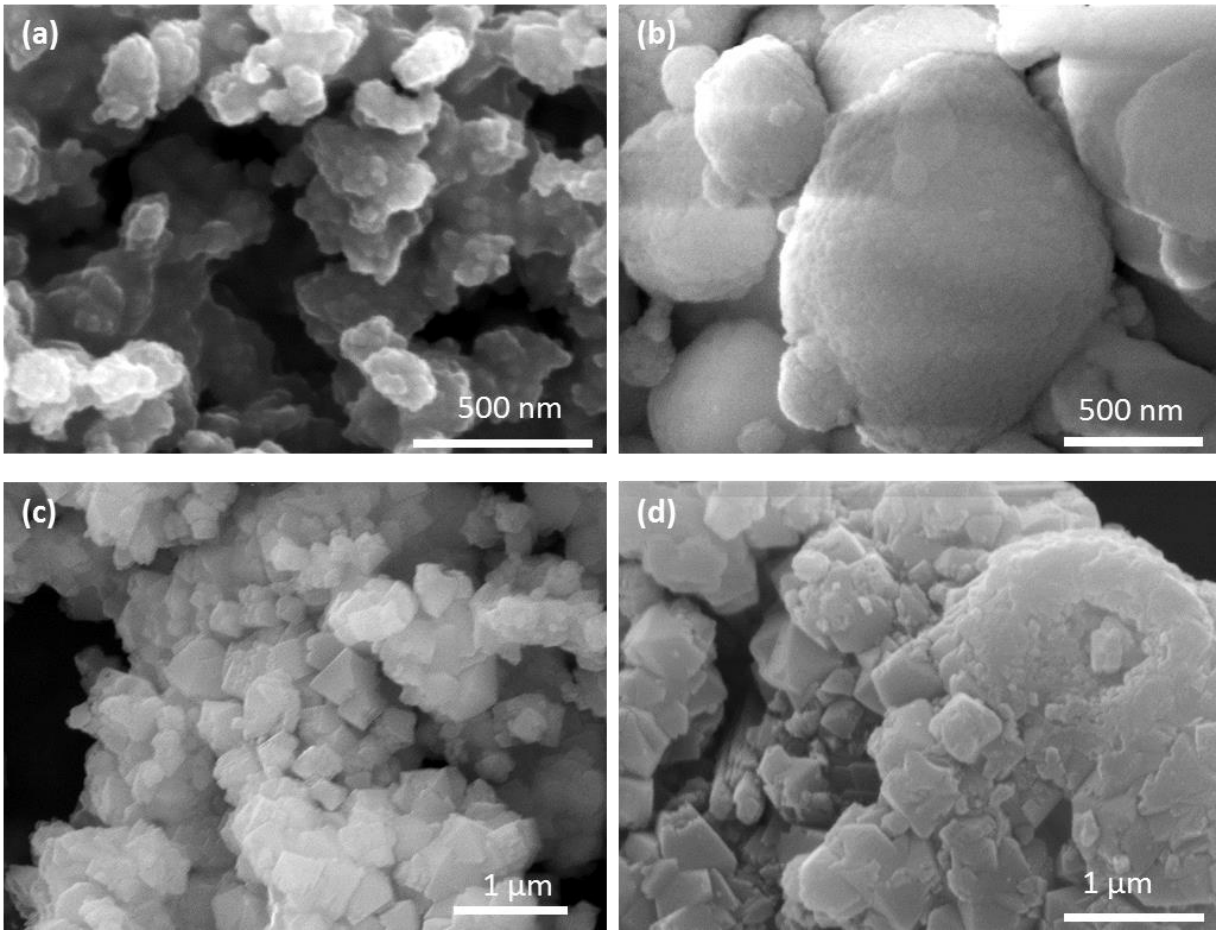

Figure 2: SEM images of Beta-1 (a), Beta-2 (b), OF-Beta (c) and OF-Beta-ST (d).

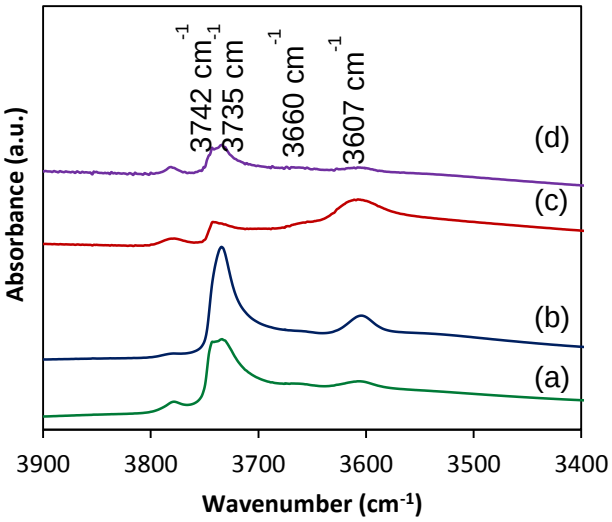

Figure 3: Infrared hydroxyl stretching region of Beta-1 (a), Beta-2 (b), OF-Beta (c) and OF-Beta-ST (d), normalized to 10 mg/cm^2.

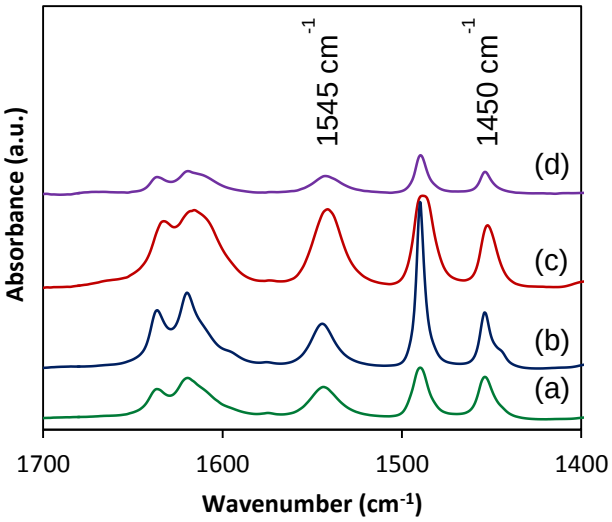

Figure 4: Difference IR spectra of adsorbed pyridine on Beta-1 (a), Beta-2 (b), OF-Beta (c) and OF-Beta-ST (d), normalized to 10 mg/cm^2. The absorption bands at 1450 cm^{-1} and 1545 cm^{-1} correspond to pyridine adsorbed on Lewis resp. Brønsted acid sites.

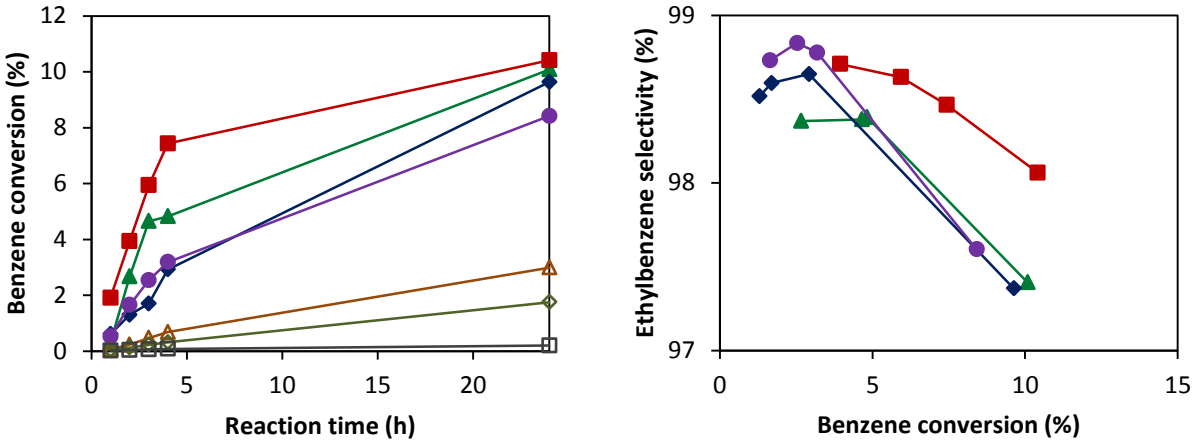

Figure 5: Benzene conversion (left) in the liquid phase alkylation of benzene with ethene (benzene : ethene 8, reaction temperature 150°C) and selectivity referred to ethene to the monoalkylated ethylbenzene for Beta-1 (▲), Beta-2 (◆), OF-Beta (■), OF-Beta-ST (●), OF-Beta-ST-0.1 (△), OF-Beta-ST-0.5 (◇) and OF-Beta-ST-6.0 (□).

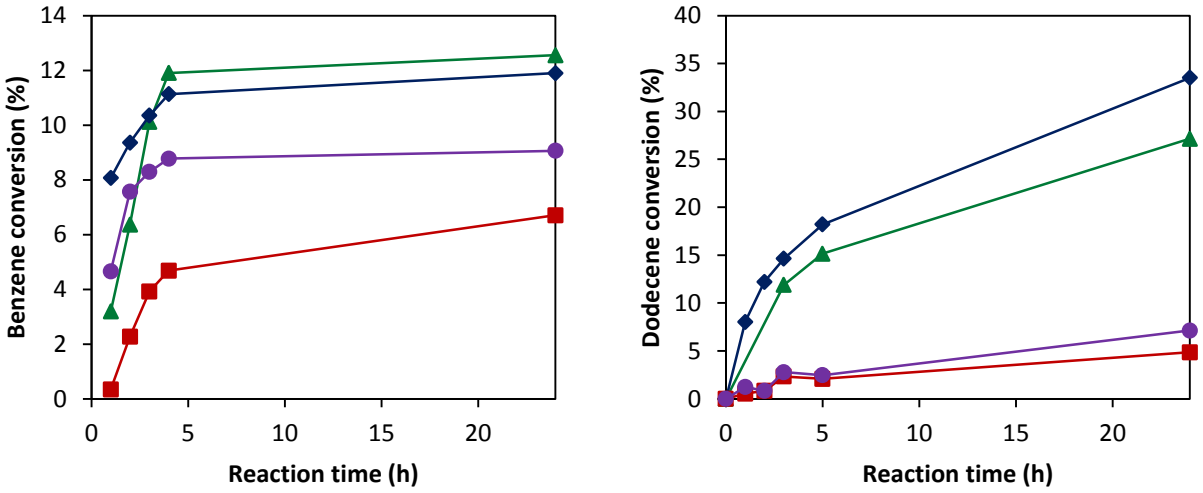

Figure 6: Benzene conversion in the liquid phase alkylation of benzene with propene (left, benzene : propene 6, reaction temperature 150°C) and dodecene conversion in the alkylation of benzene with 1-dodecene (right, benzene : 1-dodecene 8.6, reaction temperature 120°C) for Beta-1 (▲), Beta-2 (◆), OF-Beta (■), OF-Beta-ST (●).

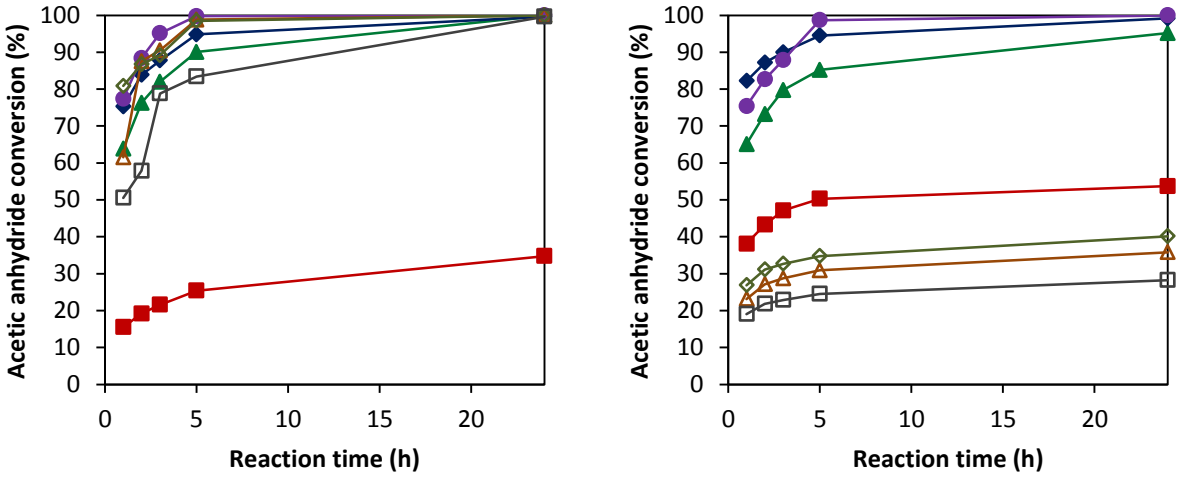

Figure 7: Acetic anhydride conversion in the acylation of anisole (left, molar ratio anisole / acetic anhydride 5) and 2-methoxynaphthalene (right, molar ratio 2-methoxynaphthalene / acetic anhydride 2) for Beta-1 (▲), Beta-2 (◆), OF-Beta (■), OF-Beta-ST (●), OF-Beta-ST-0.1 (△), OF-Beta-ST-0.5 (◇) and OF-Beta-ST-6.0 (□).

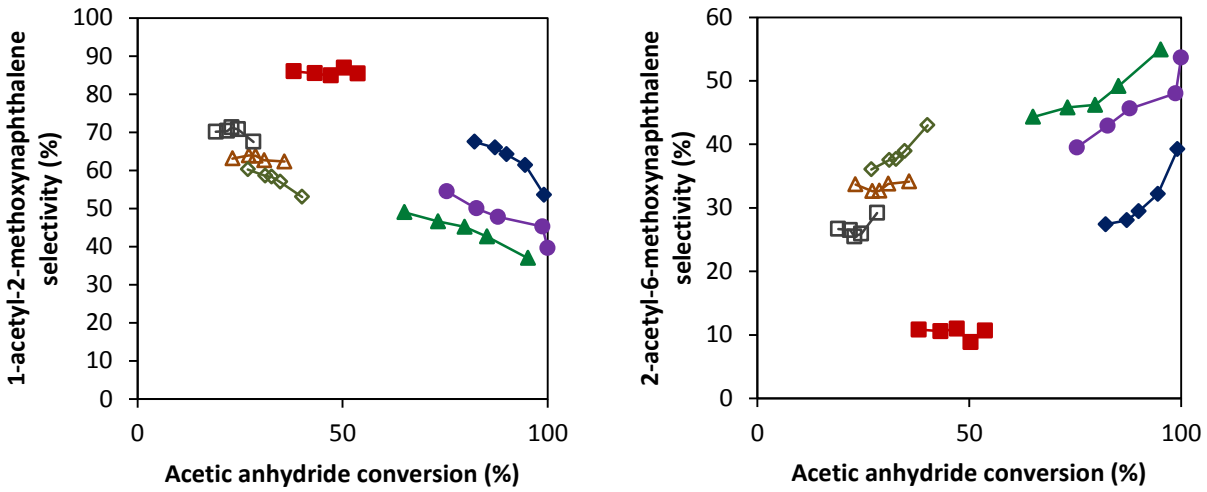

Figure 8: Selectivity to 1-acetyl-2-methoxynaphthalene (left) and 2-acetyl-6-methoxynaphthalene (right) as function of acetic anhydride conversion in the acylation of 2-methoxynaphthalene for Beta-1 (▲), Beta-2 (◆), OF-Beta (■), OF-Beta-ST (●), OF-Beta-ST-0.1 (△), OF-Beta-ST-0.5 (◇) and OF-Beta-ST-6.0 (□).

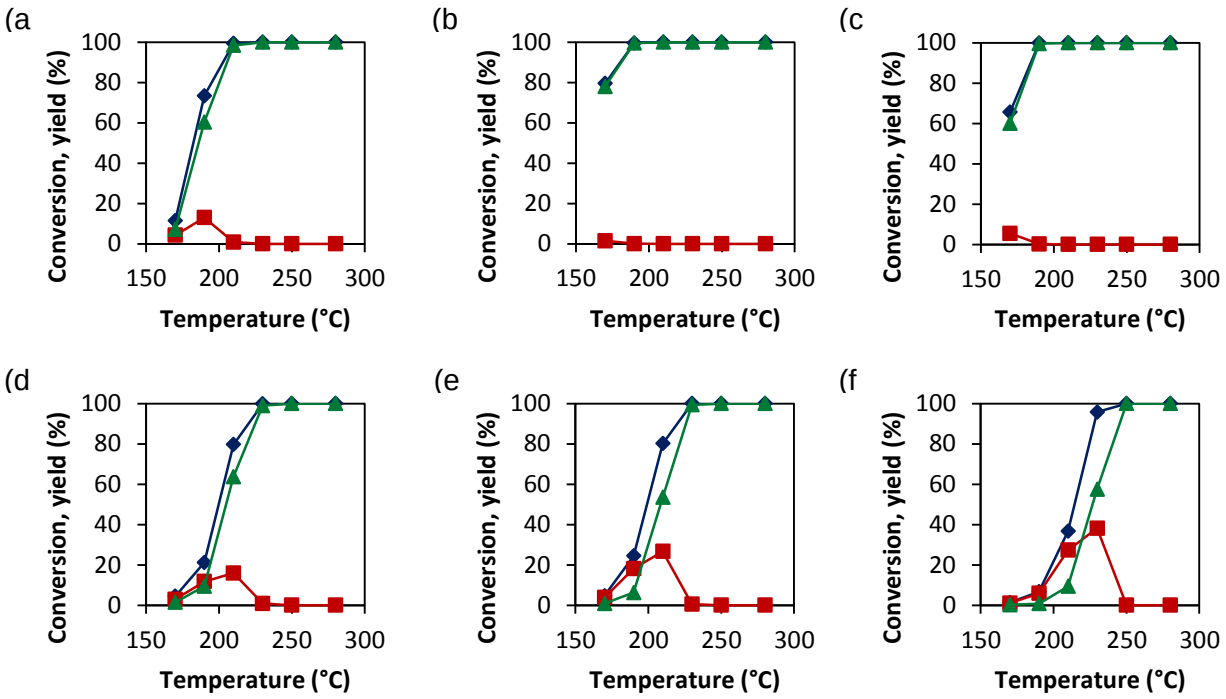

Figure 9: Catalytic results from the *n*-decane hydroconversion: *n*-decane conversion (◆), yield of isomerization products (■) and yield of cracking products (▲) for Beta-1 (a), OF-Beta (b), OF-Beta-ST (c), OF-Beta-ST-0.1 (d), OF-Beta-ST-0.5 and OF-Beta-ST-6.0 (e).

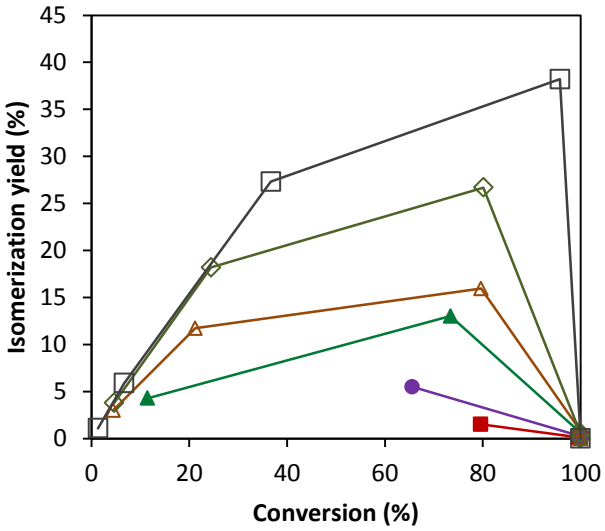

Figure 10: Yield of isomerized products as function of *n*-decane conversion for Beta-1 (▲), OF-Beta (■), OF-Beta-ST (●), OF-Beta-ST-0.1 (△), OF-Beta-ST-0.5 (◇) and OF-Beta-ST-6.0 (□).

1 List of tables

Table 1: Elemental composition and textural properties.

Sample	Si/Al[a]	Na[a] (wt.%)	V_{micro}[b] (mL/g)	V_{meso}[c] (mL/g)
Beta-1	12[d]	<0.02[d]	-	-
Beta-2	19[d]	<0.05[d]	-	-
OF-Beta	4.5	5.4[e]	0.24	<0.01
OF-Beta-ST	12.4	0.01	0.19	0.05
OF-Beta-ST-0.1	25.2	<0.01	-	-
OF-Beta-ST-0.5	36	<0.01	-	-
OF-Beta-ST-6.0	55	<0.01	-	-

[a]From bulk elemental analysis (ICP-OES). [b]Micropore volume, t-plot method. [c]Mesopore volume. [d]Data from manufacturer. [e]Before ion-exchange.

Table 2: Acidic properties determined with NH3 TPD and FTIR using pyridine as probe molecule.

Sample	B/L[a]	T_1[b] (°C)	$Peak_1$[b] (mmol/g)	T_2[c] (°C)	$Peak_2$[c] (mmol/g)
Beta-1	1.6	197	0.69	291	0.41
Beta-2	2.3	203	0.46	348	0.45
OF-Beta	3.2	208	1.99	364	1.19
OF-Beta-ST	2.4	194	0.47	333	0.37

[a]Determined from the IR absorption bands of chemisorbed pyridine at 150°C. [b]Temperature and amount of NH_3 desorbed at the first, low temperature desorption peak. [c]Temperature and amount of NH_3 desorbed at the second, high temperature desorption peak.